PHYSICAL REVIEW A VOLUME 2, NUMBER 2 AUGUST 1970

Collision Spectroscopy. III. Scattering in Low-Energy Charge-Transfer Collisions of He^+ and Ar

Felix T. Smith

Stanford Research Institute, Menlo Park, California 94025*

and

Hans H. Fleischmann†‡

Cornell University, Ithaca, New York 14850

and

Robin A. Young§

Gulf General Atomic, San Diego, California 92112

(Received 3 February 1970)

Differential charge-transfer cross sections σ are measured for He^+ in Ar at energies E from 65 to 300 eV and angles θ from 1° to 30°. The relative measurements are calibrated by comparison with total charge-transfer measurements of Koopman. From reduced plots of $\rho = \theta \sin\theta\,\sigma(\theta)$ versus $\tau = E\theta$, two, and perhaps three families of oscillations are identified, with reduced angular thresholds at $E\theta \cong 300$, 970, and 1250 eV deg and with spacing $\Delta\theta$ between peaks near threshold related to the wave number k by the rule $\Delta b = (2\pi/k\Delta\theta) \cong 0.51$, 0.25, and 0.09 a.u., respectively. Using potential curves constructed from earlier information on elastic scattering, the first family is identified as arising from a crossing at 2.9 a.u. to a state dissociating to He $(1s^2)$ + Ar^* $(3s3p^6)$, and the second from a crossing at 2.3 a.u. to a state producing He $(1s2s)$ + $Ar^*(3s^23p^5)$. Further crossings at distances between 2.25 and 1.95 a.u. leading to other excited-state channels are apparently responsible for more than half of all the charge transfer at these energies.

I. INTRODUCTION

The study of differential scattering of ions by atoms both with and without charge transfer has produced a body of very interesting information on elastic and inelastic scattering processes in recent years. The principal features of elastic scattering under these conditions are fairly well understood, and the elastic scattering curves can usually be interpreted to give specific information on the interaction potentials governing the scattering. Inelastic processes are proving to be of great importance even at energies as low as a few eV, [1] and they provide in principle further material for interpretation in terms of potential curves and other interaction parameters connecting two or more electronic states of the diatomic system which has a transient existence during the collision period. With regard to these inelastic processes we are still in the exploratory stage of progress in which various phenomena are being explored experimentally, diagnosed and classified as far as possible with respect to the nature of the interaction responsible for them, and interpreted at least semiquantitatively in the light of the developing theoretical knowledge. The goal of this type of work is to develop the principles of collision spectroscopy so that quantitative experimental data can be interpreted in terms of quantitative interaction parameters as a function of internuclear distance. [2]

Of particular value at this stage of progress is the measurement of a number of different processes involving the same colliding particles. In this situation, the different measurements can ultimately be analyzed together and used to construct a self-consistent picture of the potential curves and interactions characterizing several electronic states of the combined system.

The particular system in question here, $He^+ + Ar$, has been investigated in elastic scattering at the University of Connecticut[3] and at Stanford Research Institute, [4] and the results of these measurements have been coupled to obtain a plausible and self-consistent description of the potential curve principally responsible for the elastic scattering. [5] In addition, the elastic scattering provides some information about apparent crossings of certain potential curves and demonstrates a striking loss from the elastic scattering channels into inelastic ones, much of which is likely to be due to charge-exchange scattering. The present investigation was undertaken with these circumstances in mind and has been directed toward a measurement of the charge-transfer scattering in the same system, $He^+ + Ar$. Subsequent work at Stanford Research In-

stitute has been devoted to inelastic scattering of He^+ by Ar, and the results will be published later.[6]

A number of studies have been made of ion-atom scattering and charge transfer involving various pairs of rare-gas species, including symmetric systems[7-9] such as He_2^+, Ne_2^+, and Ar_2^+ and the asymmetric system[10] $NeAr^+$. Of special relevance here is the experimental study and analysis of the inelastic scattering of He^+ by Ne.[11] Our data analysis here is based on the methods developed in Ref. 11, and more information on the background can be obtained there.

Some of the experimental data reported on here were presented at an international conference.[12] In the present paper, we give a more detailed presentation of the experimental procedure and results, but the major emphasis is on the interpretation of the observations. Particularly important are the deductions that can be made from the characteristics of the oscillating patterns to be seen in the data. While we have made an attempt at a quantitative normalization, the absolute values of the cross sections as we estimate them are less significant than the location of the structural features which are the chief subject of our analysis.

II. BACKGROUND: DEDUCTIONS FROM ELASTIC SCATTERING

A. Potential Curves and Reduced Deflection Functions

The prior information of most value to us in this investigation is the potential-energy curves for the system $HeAr^+$ obtained through the analysis of the differential elastic scattering measurements[5] (see Fig. 1). They include the diabatic potential-energy curve for the molecular state which we have tentatively labeled $B^2\Sigma$, which is formed by bringing together the ion He^+ and the atom Ar in their ground states. The elastic scattering data can be fitted very well by using the potential function

$$V_B(r) = \frac{2e^2}{r}(8e^{-r/C_M} + 8e^{-r/C_L} + 2e^{-r/C_K}) - \frac{\alpha e^2}{2r^4} \times \left[1 - e^{-r/C_M}\left(1 + \frac{r}{C_M} + \frac{r^2}{2C_M^2} + \frac{r^3}{6C_M^3}\right)\right], \quad (1)$$

where $C_M = 0.90$ a.u., $C_L = 0.14$ a.u., $C_K \cong 0.058$ a.u., and $\alpha = 23.7$ a.u.[3] The constant α is an effective polarizability which is almost twice as great as the known polarizability of Ar (contrary to the statement in Ref. 5, where an error of a factor of 2 was committed), and the deviation apparently comes about because we are making an empirical fit to a potential which really should contain additional terms, including attractive ones of shorter range than r^{-4}. The potential of the B state can be considered to be fairly well established (with an uncertainty on the order of perhaps 1 eV or less at distances greater than about 2.5 a.u.).

We have also included on the diagram tentative guesses of the potential curves for the states $X^2\Sigma$ and $A^2\Pi$. In the absence of better information, we have estimated these curves to pass through certain points computed for the system $HeNe^+$ by Michels,[13] but scaled to slightly larger values of r by the proportionality factor $r_{Ar}/r_{Ne} = 0.90/0.70$ representing the ratio of the outer-shell screening constants for the two atoms. The X state probably lies well inside the B state at all energies of interest to us, and the A state may do so as well. Wherever the A state may lie, its interaction with the $^2\Sigma$ states is likely to be small at these energies since it is of $^2\Pi$ symmetry. We do not believe that it is responsible either for any of the perturbations observed in the B-state elastic scattering or for any important amount of charge-transfer scattering in these experiments.

In small-angle scattering ($\theta \lesssim 30°$), the most important observable is the reduced scattering angle $\tau = E\theta$, where E is the initial energy and θ is the observed scattering angle. τ is related to the impact parameter b by a functional form – the reduced deflection function – that depends on the potential (1); for elastic scattering in the B state in the region of greatest importance to us here, we can approximate τ by the form

$$\tau_B(b) \cong Ae^{-b/a}, \quad A = 5.92\times10^4 \text{ eV deg}, \quad a = 0.637 \text{ a.u.}, \quad 1.6 \lesssim b \lesssim 3.0 \text{ a.u.} \quad (2)$$

In small-angle scattering, the impact parameter b and the distance of closest approach r_0 are essentially the same, so features localized at a specific reduced angle τ_x represent interactions at some localized place $r_x \cong b_x$ on the potential $V_B(r)$.

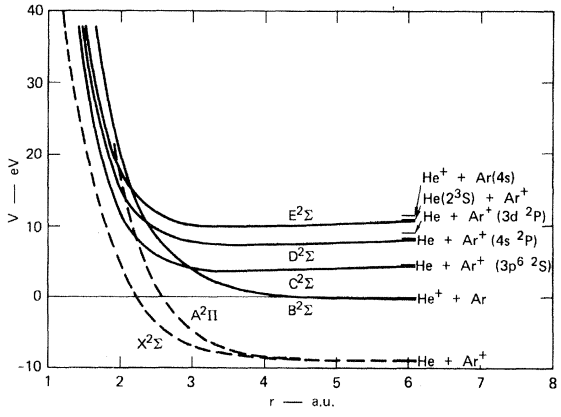

FIG. 1. Potential curves for the system $HeAr^+$.

In the elastic scattering, perturbations have been observed at certain localized values of τ, and they provide us with knowledge of the locations of the crossings of certain other potential curves with that of the B state. In particular, a perturbation apparently centered near $\tau_x = 870\,\text{eV deg} = 0.56$ a.u. rad provides evidence for a single isolated crossing at $r_{BC} \cong 2.9$ a.u. at an energy $V_{BC} \cong 4.3$ eV. This represents a crossing with a state whose symmetry is probably $^2\Sigma$ and which we label the C state; we believe it dissociates to ground-state He and an excited Ar^+ ion in the state $3p^6\,^2S$, [14] since we see no reason for it to dissociate to any higher state of Ar^+, and dissociation to any possible higher states involving either He^+ or the excited He atom would require the C state to have a dissociation energy of at least 8 eV, which seems unlikely. In the light of the elastic scattering observations, the available information on the C state comprises the approximate location of the crossing and the energy of the presumed final states after dissociation. We have used these two pieces of information to construct for the C state a plausible potential-energy curve; its form is similar to one we have found useful in the similar case of the excited states of the system $HeNe^+$:

$$V_C(r) = V_B(r) + \Delta V_{BC}(r) = V_B(r) + V_C(\infty) \times \{1 - \exp[(r_{BC} - r)/C_M]\}, \quad (3)$$

which is constructed to have the correct asymptotic energy, $V_C(\infty) = 4.7$ eV, and the correct crossing point $r_{BC} = 2.9$ a.u., and uses the same M-shell shielding constant C_M as Eq. (1). These parameters were chosen without reference to the charge-transfer data to be presented below, which will be seen to show a feature whose location confirms this identification of the BC crossing and indicates that the potential form (3) is reasonable.

A different type of perturbation in the elastic scattering, which appears as a rapid fall in the elastic cross sections over a limited region of τ, is attributed to the collective effect of losses into many inelastic channels which open up through a series of closely spaced crossings. This drop begins near the value of τ of about 1600 eV deg, which corresponds to a crossing distance of about 2.30 a.u., is falling most steeply at about 2000 eV deg where the crossing is about 2.15 a.u., and terminates at around 3000 eV deg at a crossing distance of about 1.9 a.u. Since we are interested in this paper in states from this group of crossings which dissociate to neutral He atoms and Ar ions, we have singled out and tentatively fitted two of these curves by forms of the same structure as Eq. (2). These we tentatively label the D and E states, both of symmetry $^2\Sigma$. The D state we assume to dissociate to give Ar^+ in the state $4s\,^2P$. The E state, on the other hand, dissociates to give an excited He atom and a ground-state Ar^+ ion, yielding $He(2^3S) + Ar^+$. We have arbitrarily fitted these so that the E-state crossing occurs at $r_{BE} = 2.16$ a.u., and the D state lies everywhere parallel to it with a crossing at about $r_{BD} = 2.4$ a.u. chosen so that

$$V_D(\infty) \exp(r_{BD}/C_M) = V_E(\infty) \exp(r_{BE}/C_M).$$

The asymptotic energies to be used in the potentials V_D and V_E are $V_D(\infty) = 8.43$ eV and $V_E(\infty) = 11.05$ eV.

These potential curves and a few additional doublet states of the system $HeAr^+$ are shown on a potential diagram in Fig. 1. [We omit quartet states, the first of which dissociate to $Ar^+(3d\,^4D)$ and $(4s\,^4P)$ just below the D state.] The exact shapes of the C, D, and E states are still quite uncertain, and all that is known with any certainty are the dissociation limits and some information about the crossing points with the B state.

Since these experiments give us no final velocity analysis, we can only make indirect deductions to identify the specific charge-transfer processes we may be observing. The potential-energy diagram is of great help in suggesting the likely processes and some of their properties. As already explained, we expect little or no transfer to the ground state of $Ar^+ + He$ through either the X or the A states. Because the X- and A- state potentials are both repulsive, and indeed more so than the B state if they cross it, and because any such crossing must lie rather far in, charge transfer to the ground state, if it occurs at all, would be seen only at very large values of τ, much larger than the value $\tau_x = 870$ eV deg of the outermost perturbation in elastic scattering.

The first fully available crossing from B to C provides a route for charge transfer ending with ground-state He and excited $Ar^+(3p^6\,^2S)$. Above this, a number of further excited Ar^+ states (beginning with our D state) follow with increasing rapidity, and then at 11.05 eV we encounter the E-state process involving ground-state Ar^+ and the metastable $He\,2^3S$. Dissociating $\frac{1}{2}$ eV above this is the first inelastic transition to occur without charge transfer, leading to $He^+ + Ar(4s)$.

If the potential curve for the excited state has the form of Eq. (3), the reduced deflection function for elastic scattering in the excited state can be deduced from that for the B state plus a contribution from the attractive exponential term; as an example, let us take the C-state deflection function

$$\tau_C(b) = \tau_B(b) + \Delta\tau_{BC}(b) \quad , \quad (4)$$

where the contribution from the exponential term in Eq. (3) involves the modified Bessel function $K_0(x)$:

$$\Delta\tau_{BC}(b) = -V_C(\infty)e^{r_{BC}/C_M}(b/C_M)K_0(b/C_M) \quad . \quad (5)$$

The average reduced deflection function for the BC transition is then

$$\tau_{BC}(b) = \tfrac{1}{2}\tau_B(b) + \tfrac{1}{2}\tau_C(b) = \tau_B(b) + \tfrac{1}{2}\Delta\tau_{BC}(b) \quad . \quad (6)$$

Particularly important for us is the predicted reduced threshold angle for the inelastic process, when $b \cong r_{BC}$:

$$\tau_{BC}(r_{BC}) = \tau_B(r_{BC}) + \tfrac{1}{2}\Delta\tau_{BC}(r_{BC}) \quad . \quad (7)$$

In Table I, we show a number of important properties computed for the crossings of the B state with the several states $J = C$, D, E. In the case of the C and E states, we have made some alternative assumptions about the exact location of the respective crossings with the B state, and the results show clearly the sensitivity of inelastic crossing thresholds $\tau_{BJ}(r_{BJ})$ to the location of the crossing r_{BJ}; this sensitivity arises predominantly from the repulsive B-state contribution to Eq. (7), and is not particularly sensitive to the attractive term which we have so arbitrarily given an exponential form. We also include in the table the difference in slopes of the two potentials at the crossing $\Delta V'_{BJ}$ which happens (with this choice of difference potential) to be independent of the crossing location:

$$\Delta V'_{BJ}(r_{BJ}) = V_J(\infty)/C_M \quad . \quad (8)$$

In the important C and E states we have also located the respective potential minima:

$$\begin{aligned} &V_C(\text{min}) = 3.736 \text{ eV}, \quad r_C(\text{min}) = 3.55 \text{ a.u.}, \\ &V_C(\text{min}) - V_C(\infty) = -1.0 \text{ eV}; \\ &V_E(\text{min}) = 9.966 \text{ eV}, \quad r_E(\text{min}) = 3.50 \text{ a.u.}, \\ &V_E(\text{min}) - V_E(\infty) = -1.1 \text{ eV}; \\ &V_{E'}(\text{min}) = 9.672 \text{ eV}, \quad r_{E'}(\text{min}) = 3.30 \text{ a.u.}, \\ &V_{E'}(\text{min}) - V_E(\infty) = -1.4 \text{ eV}. \end{aligned} \quad (9)$$

In the case of the C state the minimum is only 0.6 eV below the BC crossing, if the latter occurs at 2.9 a.u., and its stability is therefore in doubt. However, if the potential has the form (3), a minimum stable by more than 1 eV appears in the E state (its depth will of course depend on further improved knowledge of the potential). These minima are of some importance in connection with the possible existence of the ion $HeAr^+$ in gaseous discharges. Although $HeNe^+$ is well known and appears to be fairly strongly bound, a similar ion has never been seen in He-Ar mixtures except at exceedingly low temperatures. The known $HeAr^+$ ion is extremely weakly bound and is probably associated with the shallow polarization well in the X or A states and not with one of the excited states.[15] While it may be an experimental accident of rates and mechanism that no excited molecular ion has been seen, we think it more likely that the difference between the systems $HeNe^+$ and $HeAr^+$ is real, and that a more refined set of potential curves for $HeAr^+$ would show no minima in the excited states or that any apparently stable configurations are so perturbed by other states as to decay rapidly.

TABLE I. Properties of crossings of states $J = C$, D, and E of $HeAr^+$ with the B state.

J	$V_J(\infty)$ (eV)	r_{BJ} (a.u.)	$V_{BJ}(r_{BJ})$ (eV)	$\Delta V'_{BJ}(r_{BJ})$ (eV/a.u.)	$\tau_B(r_{BJ})$ (eV deg)	$-\frac{1}{2}\Delta\tau_{BJ}(r_{BJ})$ (eV deg)	$\tau_{BJ}(r_{BJ})$ (eV deg)
C	4.7	2.9	4.3	5.2	635	290	345
C'	4.7	2.7	6.0	5.2	870	285	585
D	8.43	2.4	10.0	9.4	1400	480	920
E	11.05	2.16	15.2	12.3	2000	585	1415
E'	11.05	2.25	13.0	12.3	1750	595	1155
E''	11.05	2.3	11.9	12.3	1600	600	1000

B. Estimation of the Coupling Matrix Element

In favorable cases, the elastic scattering data permit the measurement of additional parameters besides the crossing location, especially in the case of an isolated crossing. Thus in the case of the BC crossing at 2.9 a.u., a series of oscillations is seen in the elastic scattering pattern. These oscillations are well displayed in Figs. 6 and 8 of Ref. 5; they can be compared with similar oscillations in the He^+ scattering by Ne. Their spacing will be discussed later; here we shall be concerned with their amplitude.

In Fig. 2, we have plotted the magnitude of the elastic perturbation, measured by $\Delta\rho = \rho_{\max} - \rho_{\min}$, as a function of E, where $\rho_{\max}$ is the reduced elastic cross section at the principal maximum and $\rho_{\min}$ is taken at the valley to its left. The values are taken from Figs. 6 and 8 of Ref. 5; for comparison we present similar measurements from the elastic perturbation in $He^+ + Ne$ scattering and also the values of ρ at the leading maxima in the inelastic scattering pattern for the reaction

$$He^+ + Ne \rightarrow He^+ + Ne^*(3s), \quad \Delta E = 16.8 \text{ eV}$$

(the latter points are from Fig. 10 of Ref. 11, and only the upper envelope of that curve is used here). Although there are only 4 points in the $He^+ + Ar$ curve and the one at 200 eV is very uncertain in magnitude, the other 3 points are well reproducible, and the general agreement with the other patterns gives us reasonable confidence in the results. In the figure, the curves have been extended to reflect the facts that (a) the two curves for $He^+ + Ne$ involve the same crossing, and the amplitude of the

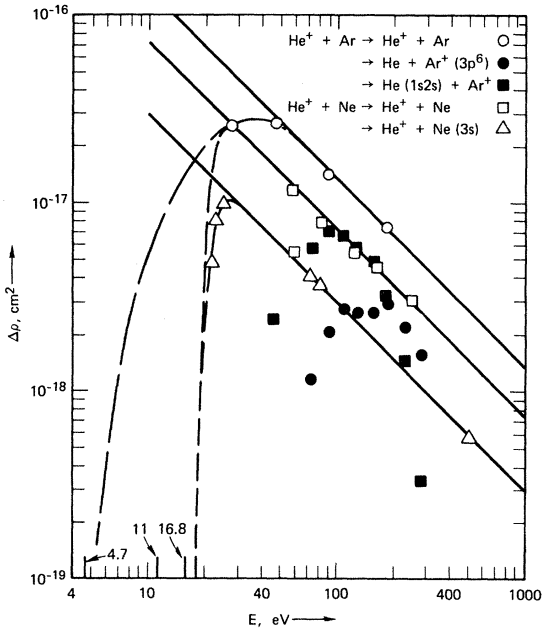

FIG. 2. Magnitude of curve-crossing interactions as a function of energy.

elastic interference pattern should have the same energy dependence as that of the inelastic pattern (as required by unitarity of the S matrix, i.e., conservation of particles); (b) the absolute thresholds for the respective processes are 16.6 to 16.8 eV for $He^+ + Ne$ and 4.7 eV for $He^+ + Ar$; and (c) the amplitudes are expected to decline as E^{-1} at high energy (see Ref. 11).

According to Fig. 2, we can estimate the maximum probability for the BC transition in $HeAr^+$ to occur at a relative collision energy of about 36 eV. Since the crossing is located at an energy of about 4 eV, this corresponds to a speed at the crossing of about 4.2×10^6 cm/sec, which is an upper bound to the radial velocity at the crossing. Assuming the maximum is described approximately by the Landau-Zener model, the characteristic Landau-Zener velocity v_{LZ} is connected with the velocity at the maximum and with the interaction parameters by the equations

$$\frac{2H_{BC}^2(r_{BC})}{|\Delta V'_{BC}(r_{BC})|} = \hbar v_{LZ} \lesssim \frac{\ln 2}{\pi}\hbar v_{max} = 0.115 \text{ eV a.u.} \quad (10)$$

Since we already have estimated $\Delta V'_{BC}(r_{BC}) \cong 5.2$ eV/a.u., we find

$$H_{BC}(r_{BC}) \lesssim 0.55 \text{ eV} \quad . \quad (11)$$

The crossing in question occurs at a fairly large internuclear distance, and the matrix element may be expected to depend strongly on the exponential tail of the Ar electron density in that region, which involves the M-shell screening length $c_M \cong 0.90$ a.u. If we express this by writing

$$H_{BC}(r_{BC}) \cong De^{-r_{BC}/c_M} \quad , \quad (12)$$

we find $D_{HeAr^+} \cong 13.2$ eV . (13)

Similar data are available for two transitions in $HeNe^+$, and the results are summarized in Table II. All three transitions can be correlated by using an expression of the form (13) for the matrix element, with a substantially constant value of D of quite a reasonable atomic magnitude. We must emphasize that all three of the matrix elements compared in Table II were obtained in a similar way, with the unknown centrifugal energy neglected, so that the estimates of D are strictly only upper bounds in each case. The relative agreement among the three magnitudes is therefore more significant than the absolute values reported.

The information we have been discussing is drawn from the locations of the maxima of the curves in Fig. 2; in addition, the absolute magnitudes of those curves are also significant. In particular, a systematic relation might be expected between the amplitudes of the elastic perturbations in $HeAr^+$ and $HeNe^+$ in the linear region of Fig. 2. For $HeAr^+$ this linear region is described by the relation

$$(E\Delta\rho)_{HeAr^+} \cong 13.6\times10^{-16} \text{ a.u.}^2 \text{ eV} \quad , \quad (14)$$

and for $HeNe^+$ the corresponding value is

$$(E\Delta\rho)_{HeNe^+} \cong 7.2\times10^{-16} \text{ a.u.}^2 \text{ eV} \quad . \quad (15)$$

$\Delta\rho$ measures the amplitude of the interference oscillations in a reduced cross section ρ that involves two scattering amplitudes, $f_B(E,\theta)$ for simple scattering in the unperturbed B-state trajectory and $f_{BCB}(E,\theta)$ for a trajectory that follows the B-state potential for $r > r_{BC}$ and the C-state potential for $r < r_{BC}$:

$$\rho(\tau, E) = \theta \sin\theta \left| p_B(E,\theta) f_B(E,\theta) + p_{BCB}(E,\theta) f_{BCB}(E,\theta) \right|^2, \quad (16)$$

where the p's are positive real coefficients related to the probabilities of following either trajectory. If we write

TABLE II. Comparison of coupling energies, $HeAr^+$, and $HeNe^+$.

System	Transition	Screening length (a.u.)	Crossing distance r_{BJ} (a.u.)	$H_{BJ}(r_{BJ})$ (upper bound) (eV)	D (upper bound) (eV)
$HeAr^+$	BC	0.9	2.9	0.55	13.2
$HeNe^+$	BC	0.7	1.9	1.0	14.5
$HeNe^+$	BD	0.7	1.23	~3.0	~17

$$\theta \sin\theta \left|f_B\right|^2 = \rho_B, \quad \theta \sin\theta \left|f_{BCB}\right|^2 = \rho_{BCB} , \quad (17)$$

and note that ρ_B varies so slowly that it can be taken as effectively constant and evaluated near the crossing point, we can write

$$\frac{\Delta\rho}{\rho_B(\tau_{BC})} \cong \left|p_B(E, \theta_{max}) + p_{BCB}(E, \theta_{max})\left[\rho_{BCB}(E, \theta_{max})/\rho_B(\tau_{BC})\right]^{1/2}\right|^2 - \left|p_B(E, \theta_{min}) - p_{BCB}(E, \theta_{min}) \times\left[\rho_{BCB}(E, \theta_{min})/\rho_B(\tau_{BC})\right]^{1/2}\right|^2 . \quad (18)$$

The upper and lower envelopes of the oscillations and the magnitude of $\Delta\rho/\rho_B(\tau_{BC})$ thus depend on the three quantities p_B, p_{BCB}, and ρ_{BCB}, all of which may vary with E and θ much more rapidly than ρ_B. However, because the crossings in $HeAr^+$ and $HeNe^+$ occur at rather different distances, a good part of the difference between the two cases shown in Eqs. (14) and (15) may be due to differences in the slowly varying component ρ_B, which is essentially independent of E in small-angle scattering. This component can be readily evaluated from our knowledge of the B-state potential in each case, and its effect removed by constructing the ratio

$$G = (E\Delta\rho)/\rho(\tau_{BC}) . \quad (19)$$

The results, presented in Table III, appear to show considerable similarity between the two systems.

C. Spacing of Oscillations in the BC Perturbation

The structure in the elastic scattering pattern due to the perturbation which we attribute to the BC crossing consists of a series of oscillations of varying amplitude which appears to be superimposed upon a broad peak followed by a single broad valley. The broad underlying structure appears to be centered at a characteristic reduced angle τ_x about midway between the wide peak and the following valley. This characteristic point on the curves occurs at a constant value of τ at all energies, and it is essentially this value of τ_x that we have used to locate the crossing point. This behavior appears to be common to the perturbations in both $He^+ + Ne$ and $He^+ + Ar$.

The oscillations superimposed on the broad structure just described are characterized by an essentially constant value of the product of the velocity and the characteristic spacing $\Delta\theta$ between peaks.

TABLE III. High energy amplitudes of elastic perturbation in $HeAr^+$ and $HeNe^+$.

System	$E\Delta\rho$ (a.u.^{2} eV)	$\rho_B(\tau_{BC})$ (a.u.^{2})	$G = E\Delta\rho/\rho_B(\tau_{BC})$ (eV)
$HeAr^+$	13.6×10^{-16}	7.1×10^{-17}	19
$HeNe^+$	7.2×10^{-16}	3.5×10^{-17}	21

These oscillations represent an interference pattern of the type predicted by Stueckelberg due to the existence of two possible trajectories inside the crossing point. The spacing of these oscillations is related to the shapes of the potential curves of the B and C states near their crossings, and particularly to features of the difference potential. It is possible to improve upon the analysis of Ref. 5 by utilizing a scaling law appropriate to small-angle scattering to describe the locations of these peaks and valleys as a function of energy and angle (see Ref. 11 for background).

In Fig. 3, the scaling law is used by plotting the peaks, numbered by integers N increasing with τ, in terms of the reduced action

$$a(\tau, E) = 2\pi\hbar(E/2\mu)^{1/2}(N - N_0) = a_0(\tau) + E^{-1}a_1(\tau) \cdots \quad (20)$$

as a function of τ. Except for the term involving the product $E^{1/2}N_0$, the data are substantially independent of E so that we can neglect $a_1(\tau)$. We can also expand $a_0(\tau)$ about the point where $a = 0$, and write

$$a_0(\tau) = A_1(\tau - \tau_0) + A_2(\tau - \tau_0)^2 \cdots . \quad (21)$$

The fact that a single pattern is expected substantially independent of energy serves to fix unambiguously the relation between the indices N at different energies; an absolute indexing of N, equivalent to determining N_0, can be sought by maximizing the overlap between the patterns at different energies. The best integral indexing is then obtained by numbering the biggest peak as $N = 1$ for $E = 91$ eV, $N = 2$ for $E = 46$ eV, and $N = 3$ for $E = 27$ eV. N_0 can still be adjusted to a noninteger value. The constants of Eq. (21) are approximately

$$\tau_0 = 0.275 \text{ a.u. rad} = 425 \text{ eV deg}, \quad A_1 = 0.79 \text{ a.u.}, \quad A_2 = -0.19 \text{ a.u.}, \quad (22)$$

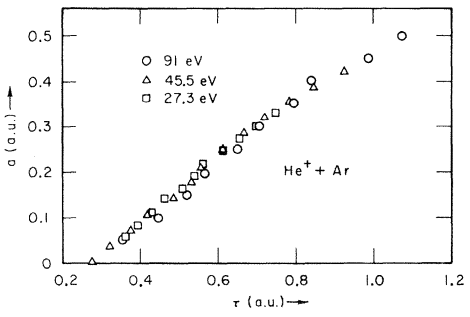

FIG. 3. Phase relations of the peaks in the elastic perturbation in the scattering of He^+ by Ar. The reduced action a is plotted against the reduced scattering angle τ.

and N_0 is close to 0; a least-squares adjustment suggests $N_0 \cong 0.25 \pm 0.40$. The fact that the constant τ_0 is significantly smaller than the value τ_x derived from the broad underlying structure is evidently no accident, since the same behavior is seen in the system $He^+ + Ne$.[11]

It is theoretically expected that the slope of the curve represented by Eq. (21) and by the data of Fig. 3 represents the difference in impact parameters between the two trajectories resulting in scattering at the reduced angle τ. This difference Δb has a maximum value of 0.79 a.u. This quantity is a significant one to compare with related information from charge-exchange scattering, since the values characterizing elastic and inelastic scattering from the same crossing are expected to be of comparable magnitude, although not identical.

III. EXPERIMENTAL DETAILS

The experimental arrangement, as shown in Fig. 4, is very similar to the one used and described earlier.[16] In short, a beam of He^+ ions is mass-analyzed and brought to the desired energy. By passage through two collimating apertures at ground potential, the angular spread of the ions entering the collision chamber is geometrically limited to about 0.5 deg, as was confirmed experimentally. The energy spread of 80% of the beam intensity at this point is about 2 eV. For small-angle measurements, the open-ended collision chamber shown in Fig. 4 was used including the connected plates for deflection and collection of the remaining ion current. From this cell, all fast helium atoms that are scattered less than 8 deg could emerge. These neutrals then were detected and counted with an open-end multiplier mounted on a movable arm, the position of which determined the scattering angle. This arm could be adjusted both in horizontal and vertical direction. Including everything, the angular resolution of this neutral detection scheme varied from 0.3 to 0.7 deg for scattering angles varying from 0 to 8 deg. For large-angle measurements, i.e., for scattering angles in the range from 4 to 32 deg, this collision chamber was replaced by a bellows cell which, on the exit side, was directly connected to the movable arm. Any scattered ions escaping through the exit slit were deflected before they could reach the multiplier entrance. The over-all angular resolution in this case was better than 0.3 deg irrespective of the scattering angle. In both cases, argon pressures in the range $3-6\times10^{-4}$ Torr were maintained in the collision chamber, and thus only single collisions were measured. In the main chamber, pressures of a few times 10^{-6} Torr prevailed.

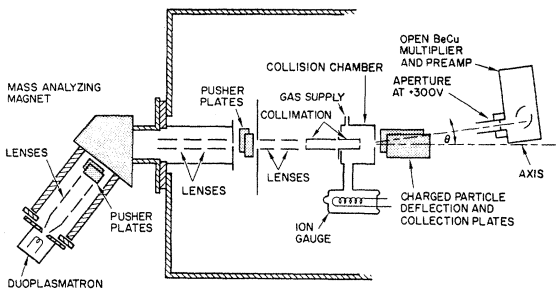

FIG. 4. Experimental arrangement.

The experimental procedures were similar to the ones described earlier.[16] For small-angle measurements, the beam axis was first determined and the horizontal position of the multiplier was adjusted correspondingly. Because of lack of charge transfer in forward scattering with the argon target, helium gas had to be introduced in the collision chamber for this purpose. For various beam parameters, the beam axis was reproducible to better than 0.3 deg, which seemed sufficient for most experiments. In large-angle measurements, the axis position could be inferred from measurements above and below the axis.

In all measurements, the angular distribution of the fast helium atoms was determined in one run over the full accessible range of scattering angles. Between several hundred and 10^5 pulses were counted in each position. Because of the small total cross section of the investigated reaction and the comparatively wide angular distribution, the fast neutrals produced either in the beam duct before the collision chamber or by neutralization with the background gas or with metal parts in the chamber itself gave a background count rate considerably more significant than in our earlier measurements. Therefore, in a number of positions, three additional count rates were determined: C_1, when the ion beam was stopped before the collision chamber by applying a suitable potential to the entrance aperture; C_2, when the argon flow to the chamber was stopped; and C_3, when both procedures were applied. The background count rate then was taken as $C_1 + C_2 - C_3$. It proved to be strongly dependent on the beam tuning, which therefore had to be optimized before each experimental run. In the final measurements, this background generally accounted for less than 15% of the total count rate for scattering angles $\theta > 2-4$ deg, but it increased very rapidly at smaller angles and thus limited the range of angles where useful measurements could be made. At the lowest angles for which measurements are reported here, the background rate was typically 70–80% of the total count rate and variations in

ion current or beam direction occurring between measurements of signal and background could produce significant variations in net signal. Thus, the experimental uncertainty may be up to 30% in these cases, but should decrease rapidly for larger angles.

As usual, the signal counts derived by subtracting the background rate were normalized to the ion current. From these numbers, the angular distributions for large- and small-angle measurements were derived and the two parts were fitted together in the overlap region $4 < \theta < 8$ deg. Except for the points closest to the beam axis, the statistical error generally is smaller than 3% and we would expect an experimental precision of about 10–15% for the over-all distributions.

The resulting relative differential cross sections are shown in Figs. 5 and 6. The experimental points shown give an indication of the scatter of the data and of the fitting between the small- and large-angle measurements. Representative estimates of total errors from counting statistics and background subtraction are indicated in several places.

Because of the large width of the distributions, for most of the curves no absolute values can be derived for the differential cross sections. However, for a beam of 300 eV, the relative cross section at 30 deg is sufficiently small to expect that most of the helium atoms are scattered less than that angle, and therefore a comparison with the total cross section can be made. Using Koopman's value, [17] we then obtain a differential cross section of about 1.6×10^{-14} cm^2/sr at the maximum of the 300-eV curve. Because of the omission of the high-angle scattering, this result is an upper bound. This assumes equal detection efficiencies for He in the ground and excited states, which seems reasonable at 300 eV. [18]

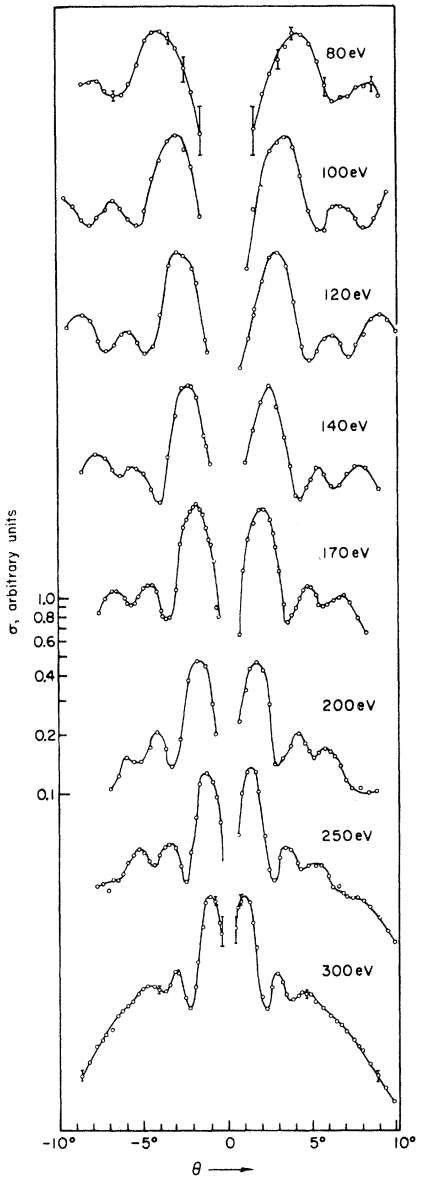

FIG. 5. Experimental results, small-angle scattering. Differential cross sections σ are plotted against scattering angle θ for different laboratory energies E_L.

IV. ANALYSIS AND DISCUSSION

A. Qualitative Observations

The experimental data of Figs. 5 and 6 show an absence of charge-transfer scattering in the forward direction and its inception at a comparatively clearly marked threshold region at finite angles, followed by an oscillating structure at larger angles. The data from 80 to 300 eV displayed in Fig. 5 have their first maximum characterized by an essentially constant value for the reduced angle of $\tau = E\theta$ at about 335 eV deg. The data at 50 and 65 eV displayed in Fig. 6 show no detectable peak in that region, but they clearly show a broader peak at larger angles characterized by a reduced angle at the maximum of $\tau = \sim 1090$ eV deg; a peak with these characteristics is also observable at higher energies. As a more thorough analysis shows, each of these two peaks is the first member of a regularly spaced set of oscillations, and the two sets of oscillations are often superimposed. As a first approximation, we can measure the threshold of each set of oscillations by the location of the first maximum in the cross section curve, as expressed in the reduced angle $\tau = E\theta$. The threshold value of $\tau_{max} \cong 335$ eV deg for the oscillations at small angles leads us to identify this structure with the BC crossing, whose predicted threshold is 345 eV deg (see Table I).

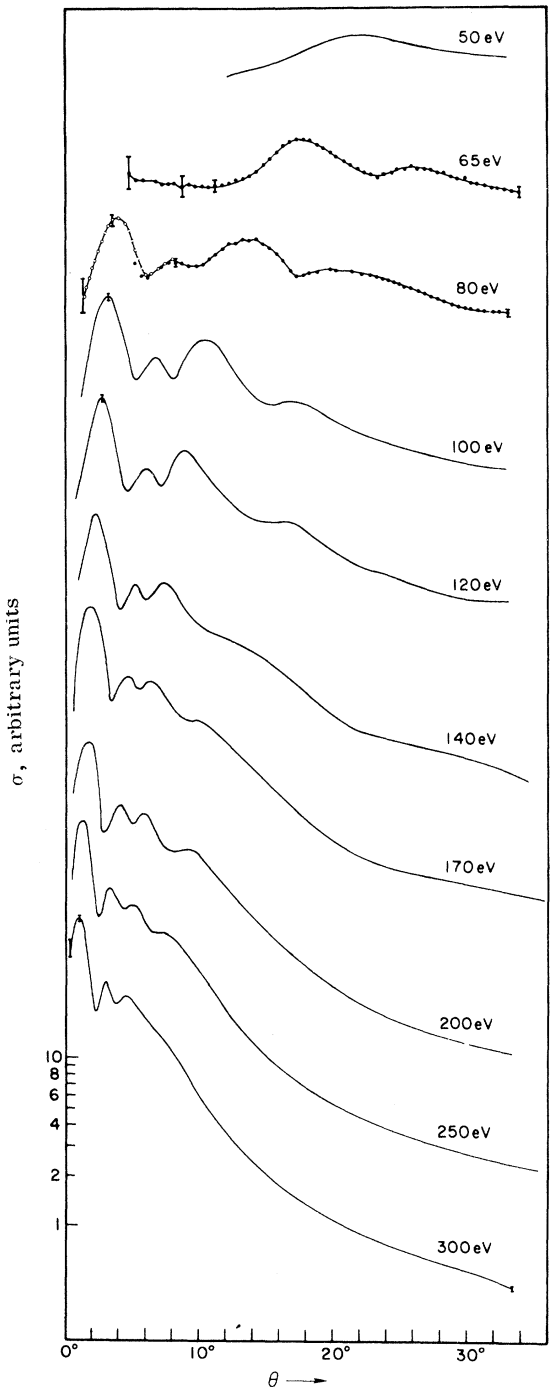

FIG. 6. Experimental results, large-angle scattering. Differential cross sections σ are plotted against scattering angle θ for different laboratory energies E_L.

It is significant that the apparent cross section for this $B \rightarrow C$ transition appears to drop off rapidly with energy below 100 eV, so that the peaks in the scattering pattern attributable to this process are rather small at 80 eV and undetectable at 65 eV. This behavior contrasts strongly with that of the related perturbation in the elastic scattering, which has its greatest amplitude between 35 and 40 eV. This effect is not altogether surprising, since the C state dissociates to produce He in the ground state, and the efficiency of this species in ejecting electrons from the detector declines rapidly at these energies.

In striking contrast, the experimental measurements at 50–80 eV show the second set of oscillations giving strong signals at energies where the first set is becoming undetectable. This implies that the neutral He atom seen in these peaks is being produced in a metastable state, since metastables are known to have a high coefficient for electron emission from solid surfaces even at very low energies. (Confirmatory evidence for such electron ejection by He metastables is seen in experimental measurements on differential charge transfer in the system $He^+ + He$.[19] At 100 eV a very considerable nonoscillatory component is found which is not due to the oscillations of the ground-state charge-transfer process.[7] This underlying contribution occurs in regions of angle and energy where inelastic scattering measurements show that He metastables are indeed produced.[20])

The second set of oscillations, like the first, appears to obey reasonably well the rule of an approximately constant value of τ at the first maximum, the average value being about 1090 eV deg.

As shown in Fig. 1 and Table IV, the E state is the first available one dissociating to give an excited neutral He. It (or higher states) must therefore be responsible for the observed signal at 65 eV, and for the second set of oscillations in general. Other states, including the D state which produces unex-

TABLE IV. Some dissociated energy levels of $(HeAr)^+$ (energies measured from the ground state of $He^+ + Ar$).

Atomic states	Energy	Molecular states
$He(^1S) + Ar^+(3p^5\,^2P^0)$	− 8.82	$X\,^2\Sigma$, $A\,^2\Pi$
$He^+(^2S) + Ar(^1S_0)$	0	$B\,^2\Sigma$
$He(^1S) + Ar^+(3p^6\,^2S)$	4.65	$C\,^2\Sigma$
$He(2\,^3S) + Ar^+(3p^5\,^2P^0)$	10.98	$E\,^2\Sigma$
$He(2\,^1S) + Ar^+(3p^5\,^2P^0)$	11.77	
$He(2\,^3P) + Ar^+(3p^5\,^2P^0)$	12.11	
$He(2\,^1P) + Ar^+(3p^5\,^2P^0)$	12.38	
$He^+(^2S) + Ar(4s,\ J=2)$	11.54	$E\,^2\Sigma$
$He^+(^2S) + Ar(4s,\ J=1)$	11.61	
$He^+(^2S) + Ar(4s',\ J=0)$	11.72	
$He^+(^2S) + Ar(4s',\ J=1)$	11.82	
$He(1^1S) + Ar^+(4p^2D^0)$	10.9	
$He(1^1S) + Ar^+(4p^2S^0)$	11.14	

cited He, and states higher than the E state which may produce excited or unexcited He, may also participate in the cross sections observed, particularly at energies above 150 eV. Since many of these states lie close to each other, it is unlikely that individual sets of oscillations due to separate states will be resolvable.

B. Reduced Variables and Normalization

In order to analyze these experimental results more closely, we have recomputed them in terms of the reduced scattering angle τ and the reduced cross section

$$\rho = \theta \sin\theta \, \sigma(\theta, E). \tag{23}$$

The resulting curves are shown in Fig. 7, tentatively normalized as described below. These curves show prominently the two sets of oscillations described above, but they show much more clearly than the cross-section data themselves that these oscillations are superimposed upon a much broader structure (with one or two maxima), which we attribute to the cumulative effect of crossings into many excited molecular states other than the C and E states. We have arbitrarily introduced in Fig. 7 an underlying smooth curve $\rho_1(\tau, E)$ which we tentatively attribute to the higher excited states in question. By subtraction, we can obtain the oscillating portions attributable to the C and E states; these are presented in Fig. 8.

Three features of the reduced cross-section curves are worthy of remark. First, the curves at the highest energies, 200 eV and above, appear to be extrapolating almost horizontally as τ increases to larger and larger values. Second, in the energy range above 140 eV, where the first maximum of the underlying broad structure is well defined, it appears that the ratio between the peak height and the maximum slope of the underlying structure in the region to the left of the peak is almost independent of energy. Third, in the same energy range, the ratio between the first peak height of the broad structure and its succeeding minimum is almost constant. The latter two ratios are shown in Table V. These characteristics of the underlying pattern suggest that there may be some very rough similarity principle that can be used to attempt to predict shapes of the curves at lower energies and to extrapolate them to larger values of τ. The existence of a second peak in the underlying structure from 100–170 eV and the suggestion that this second peak is moving up toward the first one in the data at 120 and perhaps 100 eV means that this similarity of behavior is very imperfect. We have, nevertheless, attempted to employ it in order to obtain a tentative normalization of the curves shown in Fig. 7.

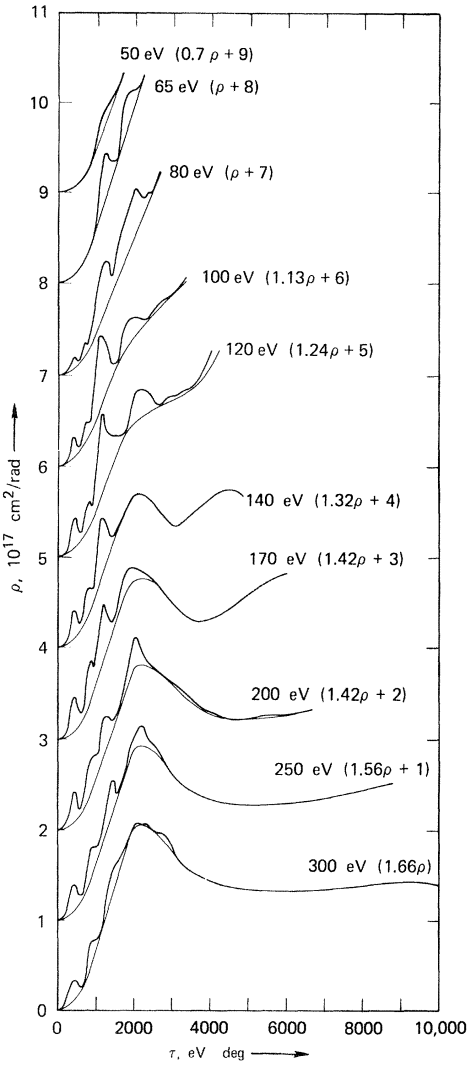

FIG. 7. Reduced cross sections ρ (heavy curve) as a function of reduced angle τ for various laboratory energies E_L. The light curve represents ρ_1, an estimate of the reduced cross section arising from states other than C and E.

In order to accomplish this normalization, we have employed the fiction that the shape of the underlying smooth curve at τ values larger than its first maximum at about 2200 eV deg is similar to the curve at 300 eV, and that it ultimately extrapolates at a constant value toward larger values of τ. Using this assumption for the extrapolation of the curves at low energies, and adding to this underlying shape the oscillating portions, it is possible to obtain for each of the curves an estimated total cross section

$$S(E) = 2\pi \int_0^{\pi} \theta^{-1} \rho \, d\theta \,. \tag{24}$$

This estimated total cross section can be compared with the experimental measurements of Koopman[17]

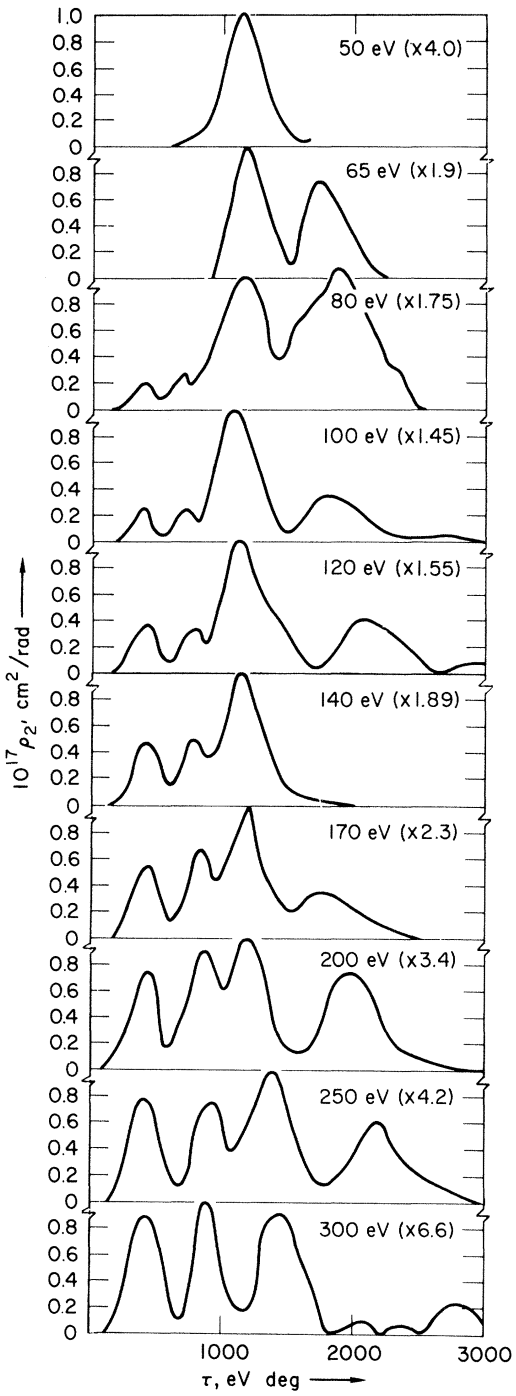

FIG. 8. Estimated reduced cross sections ρ_2 for charge transfer into the C and E states.

in order to normalize the reduced cross sections; at energies above 140 eV the reduced cross section was normalized at the maximum of the underlying smooth curve in Fig. 7, and at lower energies the slope of the initial linear rise was the basis of normalization. At 300 eV, we believe the normalization is probably reliable to about 50%, since the extrapolation of ρ from 33° to 180° contributes almost one-half of the total in Eq. (24); the normalization becomes more and more speculative at lower energies, and below 150 eV the error is likely to be as much as a factor of two or three and may be still greater. (At the lower energies, of course, a single normalization is of limited value, because the curves are sums of contributions from both ground-state and metastable He, each of which has a different secondary emission coefficient when it encounters the detector.)

We have included in Table V further details relevant to the normalization. We define $\rho_1(\tau, E)$ as the smooth underlying curves sketched in Fig. 7, so that Fig. 8 represents the difference

$$\rho_2(\tau, E) = \rho(\tau, E) - \rho_1(\tau, E). \tag{25}$$

To effect the normalization we assumed that we could approximate $\rho_1(\tau, E)$ at all energies by $\tilde{\rho}_1(\tau)$, which is defined to be equal to $\rho_1(\tau, 300\text{ eV})$ extrapolated horizontally to larger τ. The total cross section $S(E)$ was taken as the sum of two terms

$$S(E) = S_1(E) + S_2(E), \tag{26}$$

where we assumed

$$S_1(E) = 2\pi \int_0^{E\pi} \tau^{-1} \tilde{\rho}_1(\tau)\, d\tau, \tag{27}$$

and computed

$$S_2(E) = 2\pi \int_0^{\tau_2(E)} \tau^{-1} \rho_2(\tau, E)\, d\tau \tag{28}$$

directly from the data of Fig. 8, using an appropriate upper limit $\tau_2(E)$ near 3000 eV deg at all energies. We have also estimated the apparent total cross section $S_C(E)$ of the C-state process by integrating out to the region where the E-state peaks become important; this is an underestimate, since all the rest of the oscillations are assumed to belong to the E state (except at 300 eV, where the C state clearly dominates at all angles).

C. C-and E-State Oscillations

The subtraction of the smoothly varying background brings out the principal oscillating structures particularly clearly. The locations of maxima and minima are especially easy to measure, and the heights of the maxima can be reasonably well measured at least insofar as they exceed the minima. However, the arbitrariness of the subtraction particularly affects the heights of the minima, and it is impossible to estimate just what these should be, although an examination of inelastic scattering in similar systems[11,20] shows that

TABLE V. Properties of the reduced cross section.

E_L (eV)	$\rho_1(\max)/\left(\frac{d\rho_1}{d\tau}\right)_{\max}$ (eV deg)	$\frac{\rho_1(\max)}{\rho_1(\min)}$	$\frac{S_1(E)}{\rho_1(\max)}$	$\frac{S_2(E)}{S_1(E)}$	$\frac{S_1+S_2}{\rho_1(\max)}$	$S(E)$ [a] (10^{-16} cm^2)	$\frac{S_C(E)}{S_2(E)}$	$\frac{S_C}{S_2-S_C}$	$E\rho_C(\max)$ (10^{-16} cm^2 eV)	S_C 10^{-17} cm^2	S_E 10^{-17} cm^2
50			7.21	0.03	7.44	1.66	0	0	0	0	0.5
65			8.25	0.09	9.02	1.67	0	0	0	0	1.4
80			9.15	0.26	11.52	1.68	0.19	0.23	8.3	0.7	2.8
100			10.08	0.20	12.05	1.70	0.31	0.45	16.4	0.9	1.9
120			10.83	0.23	13.33	1.72	0.39	0.64	26	1.3	2.0
140	1.32×10^3	1.28	11.48	0.16	13.28	1.74	0.60	1.5	31	1.4	1.0
170	1.30×10^3	1.37	12.28	0.16	14.20	1.78	0.60	1.5	37	1.5	1.0
200	1.48×10^3	1.49	12.95	0.14	14.82	1.82	0.58	1.4	48	1.3	0.9
250	1.44×10^3	1.51	13.88	0.10	15.24	1.87	>0.5	> 1	42	0.9	0.8
300	1.39×10^3	1.55	14.63	0.07	15.70	1.93	>0.9	>10	37	1.1	0.1

[a]Reference 15

the minima generally do not approach zero and may be close to one-half the height of the neighboring maxima. Thus, our subtraction may have attributed somewhat too much to higher states and somewhat underestimated the C- and E-state cross sections which are apparently the dominating contributions to the curves of Fig. 8.

In Fig. 8, the C-state oscillations are seen to begin with a maximum at about 400 eV deg and the succeeding peaks and valleys are approximately equally spaced. We have numbered the peaks with successive integers N (beginning with $N=0$) and the valleys with half integers, and we have assumed that $N=-\frac{1}{4}$ at the half-way point of the initial rise. Following the scaling law of Eq. (20), we have plotted in Fig. 9 the quantity $NE^{1/2}$ versus τ. The E-state peaks and valleys can be numbered in the same way, and they too are included in the same plot. As Fig. 9 shows very clearly, the two families of peaks and valleys are quite distinct and fall into well-behaved patterns than can be described by Eqs. (20) and (21). The curve for the C state is essentially linear, and the apparent jog in it in the neighborhood of 900 eV deg is clearly an artifact arising from the measurement of the peaks and valleys of the C-state pattern where they are superimposed on the initial rising portion of the first E-state peak; in this region, C-state peaks are shifted to the right and valleys to the left. The C-state pattern can be parametrized in

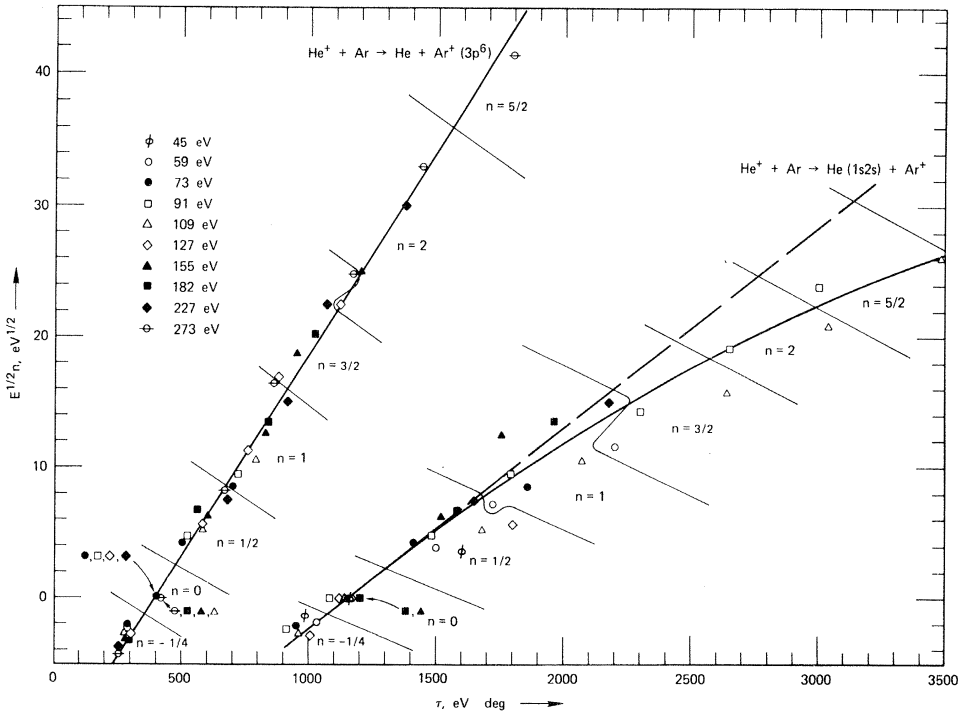

FIG. 9. Phase relations of the peaks in C and E states. $NE^{1/2}$ plotted against τ, where $N=n$ is an index number for the peak and E is the c.m. energy.

the form

$$NE^{1/2} = 30.8 \times 10^{-3}(\tau - 400), \quad (\text{eV, deg}) \qquad (29)$$

where E, the c.m. energy, is measured in eV and τ is measured in eV deg.

The E-state pattern has an initial slope about half of that for the C state, and shows a distinct falling off in slope at large values of τ. It is reasonably well parametrized as

$$NE^{1/2} = 15.4 \times 10^{-3}(\tau - 1150) - 1.76 \times 10^{-6}(\tau - 1150)^2. \qquad (30)$$

As Eq. (20) shows, the true reduced variable to be used in a plot like Fig. 9 is not necessarily proportional to $NE^{1/2}$, but to $(N - N_0)E^{1/2}$, where N_0 is a constant smaller than 1. According to Thorson and Boorstein,[21] for the inelastic scattering, $N_0 = -\frac{1}{4}$, and this value has been confirmed experimentally[11] by measurements in the system $He^+ + Ne$. It is a consequence of very general principles, based on the conservation of particles and the consequent unitarity of the quantal S matrix,[22] that the elastic and inelastic values of N_0 are related by the equation

$$N_0(\text{el}) - N_0(\text{inel}) = \tfrac{1}{2}. \qquad (31)$$

Thus, we expect $N_0(\text{el}) = \frac{1}{4}$, consistent with the data given below Eq. (22). The Thorson-Boorstein prediction can be tested by plotting the value of τ at the first maximum, where $N = 0$, against $E^{1/2}$; the slope of the resulting curve should be proportional to N_0. Such plots for the C- and E-state data are shown in Fig. 10, where the lines drawn represent the assumption $N_0 = -\frac{1}{4}$. Although the data scatter very broadly, they are clearly consistent with the Thorson-Boorstein prediction.

Further substantiation of the value $N_0(\text{inel}) = -\frac{1}{4}$ is seen in the fact that the lines in Fig. 10, which are drawn with the predicted slopes and placed to run through the center of the experimental pattern, extrapolate to the respective intercepts

$$\tau_C(E = 0) \cong 320 \text{ eV deg}$$

and

$$\tau_E(E = 0) \cong 970 \text{ eV deg},$$

agreeing very well with the average location of the points assigned the value $N = -\frac{1}{4}$ in Fig. 9. We conclude therefore that the threshold of the pattern is best located at that point, half-way up the rise to the first peak. This implies that the crossings are at

$$r_{BE} \cong 2.31 \text{ a.u.} \quad \text{and} \quad r_{BC} \cong 2.92 \text{ a.u.}$$

We can accordingly replace Eqs. (29) and (30) by a new fit:

$$(N_C + \tfrac{1}{4})E^{1/2} = 31.4 \times 10^{-3}(\tau - 300), \quad (\text{eV, deg}) \qquad (32)$$

$$(N_E + \tfrac{1}{4})E^{1/2} = 15.4 \times 10^{-3}(\tau - 970) - 1.64 \times 10^{-6}(\tau - 970)^2, \qquad (33)$$

where the units are again eV and deg. Following Eq. (20) and converting to a.u. and rad, we have

$$a_C(\tau, E) = 2\pi\hbar(E/2\mu)^{1/2}(N_C + \tfrac{1}{4}) = 0.51 \text{ a.u.}\ (\tau - 0.1925)(\text{a.u., rad}), \qquad (34)$$

and similarly

$$a_E(\tau, E) = 0.25(\tau - 0.622) - 0.042(\tau - 0.622)^2, \ (\text{a.u., rad}). \qquad (35)$$

In principle, the reduced action $a(\tau, E)$ may depend on E^{-1} as indicated in Eq. (20), but such a dependence does not seem to be significant at the energies studied here.

The slope of the curves in Fig. 9 $\partial a/\partial\tau = \Delta b(\tau, E)$ is particularly important because it provides a direct measure of the difference in impact parameters leading to scattering at the same angle from the two trajectories that create the interference pattern. In the C state, the function $a_C(\tau)$ is essentially linear over the range of τ observed, and we have

$$\Delta b_C(\tau, E) = 0.51 \text{ a.u.} \qquad (36)$$

This is to be compared with the relationship obtained from the elastic perturbation by Eqs. (21) and (22),

$$\Delta b_C(\text{el}) = 0.79 - 0.38(\tau - 0.275), \ (\text{a.u., rad}); \qquad (37)$$

just as in the case of $He^+ + Ne$[11] the threshold value of Δb is somewhat higher in the elastic case than in the inelastic one. In the E state, in contrast,

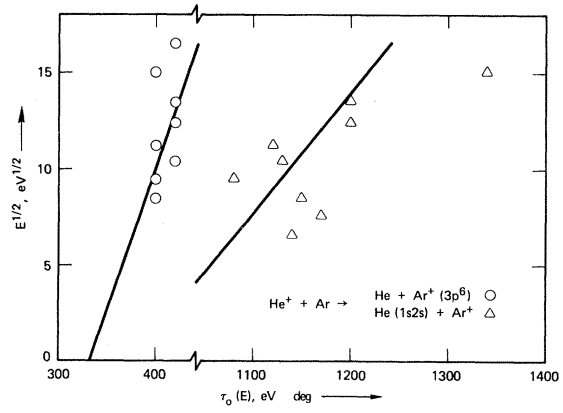

FIG. 10. Threshold behavior of the C- and E-state oscillations. τ_0 is the location of the first peak. Lines correspond to the theoretical value $N_0 = -\frac{1}{4}$.

$a_E(\tau)$ is significantly nonlinear and we have

$$\Delta b_E(\tau) = 0.25 - 0.082\,(\tau - 0.622), \quad \text{(a.u., rad)}. \quad (38)$$

Thus Δb_E declines from 0.25 a.u. at threshold to about 0.12 a.u. at

$$\tau = 2.25 \text{ a.u. rad} = 3500 \text{ eV deg}.$$

A gradual decline in Δb toward larger τ is expected, since the two interfering branches of the reduced deflection τ must approach each other as τ increases. As the respective impact parameters both decrease, so must the difference between them.

The fact that Δb_E is considerably smaller than Δb_C is understandable from the same physical argument. The BC crossing occurs at a larger internuclear distance than the BE crossing (Table I), so that larger impact parameters are available in the C state and a larger Δb is possible. In addition, the C state inside the crossing is less repulsive than the E state, so the two branches of the deflection function deviate further from each other in the C than in the E state.

D. Amplitudes in the C and E States

It is most convenient to measure the amplitudes of the C- and E-state oscillations by the height of the first maximum in each pattern. These are plotted in Fig. 2 where they can be compared with the magnitudes of the elastic perturbation and with similar data for the system $He^+ + Ne$.

The C-state charge transfer arises from the same crossing that is responsible for the elastic perturbation in $He^+ + Ar$, and the amplitudes of these two corresponding sets of oscillations are expected to be roughly proportional to each other, as they are in the similar case of $He^+ + Ne$. This means that the C-state charge-transfer amplitude is expected to be inversely proportional to the energy throughout the range of these observations. In fact, the apparent amplitudes fall off rapidly at lower energies. We attribute this fall off mostly to the decreasing efficiency of ground-state He atoms in ejecting electrons from the target as the energy declines. We show in Fig. 11 a coefficient α as a function of the laboratory energy E_L, where α is taken as the ratio of the observed C-state amplitude to the value expected from a simple E^{-1} extrapolation of the high-energy points. This coefficient depends to an unknown degree on errors in calibrating the cross sections, which we expect to cause only a rather gradual shift in magnitude, and on the ratio of the detection efficiency for He in the ground state and in the metastable states. It is the latter ratio that we believe to be responsible for the major part of the decline in the observed coefficient α, which drops by about a factor of 5 between 200 and 80 eV, and considerably further by 65 eV.

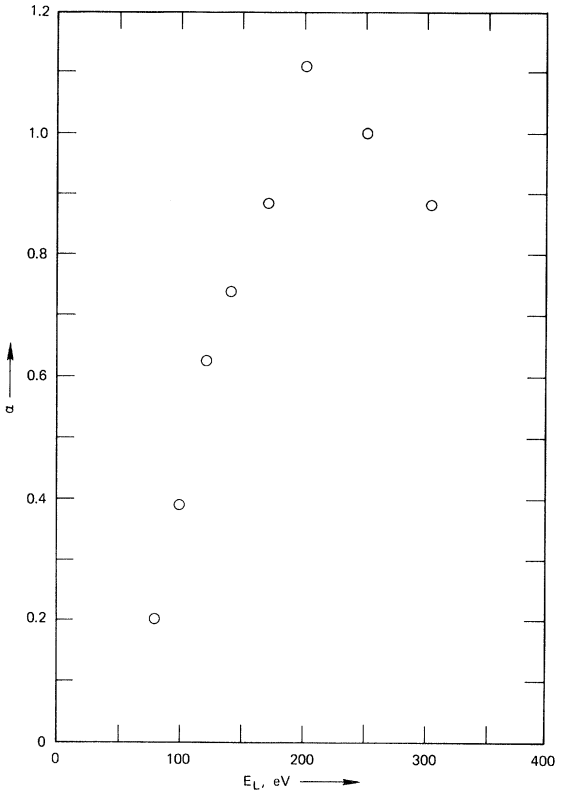

FIG. 11. Low-energy fall off of the apparent C-state amplitude. The coefficient α represents the product of an unknown calibration error and the ratio of secondary-emission coefficients for ground-state and metastable He on the solid detector surface.

The E-state amplitude is easily measured at low energies where the apparent C-state amplitude is comparatively small. At energies around 200 eV, there is some uncertainty in the measurement because of the overlapping of the two patterns, but it is particularly valuable to observe the height of the C-state minimum occurring between 1000 and 1100 eV deg. This minimum is raised above its neighbor to the left because of the underlying E-state peak, and is therefore helpful in evaluating the height of that peak. It is noteworthy that the E-state peak appears to decline rapidly in amplitude at energies above 200 eV and appears to be only about 15% of the height of the C state at 300 eV.

The exact values of the E-state amplitude must be considered uncertain because of calibration errors, variations in detector efficiency, and uncertainties in the subtraction leading to the curve of Fig. 8; nevertheless, the general shape represented by the E-state data in Fig. 2 and the relative changes in amplitude are believed to be fairly reliable. Clearly the E-state amplitude declines at

energies above 200 eV at a rate much faster than the ordinary E^{-1} behavior would indicate, and we believe this decline is due to a superimposed oscillation of the type that is also seen in the inelastic scattering of He^+ by Ne in the 3s state. In the latter case the explanation appears to be an oscillation between the two sets of products $He^+ + Ne$ (3s) and $He(1s2s) + Ne^+$, which happen to be almost degenerate energetically. In the present case, as Table IV shows, there is a similar near degeneracy involving the two possible sets of products $He^+ + Ar$ (4s) and $He(1s2s) + Ar^+$, and there is even a third set $He(1s^2) + Ar^+(4p)$. Depending on phase relations as a function of impact parameter and energy, either one or another of the three possible products may be favored. Similar oscillations in amplitude are therefore expected in the inelastic scattering of He^+ by Ar, producing Ar(4s). In contrast, there is no available inelastic channel without charge transfer anywhere near the dissociation limit of the C state, and that state does not appear to show a significant amplitude oscillation of this type. The deviation at high energies from $E\rho_C \cong$ const do not exceed the uncertainty of normalization.

The effects we have seen in examining the amplitudes of the first peak of each pattern are also seen in the total cross sections, which are at least crudely estimated by the quantities S_C and $S_E = S_2 - S_C$, tabulated in Table V. At energies between 120 and 200 eV the total cross sections for the two states are roughly comparable in magnitude. At lower energies, the apparent C-state contribution falls, undoubtedly because of reduced detection efficiency, and at energies above 200 eV the E-state contribution falls, probably because it is dissociating predominantly in the inelastic scattering mode rather than in the charge-transfer mode. This decline in the observed E-state charge transfer is perhaps also involved in the decline in the ratio S_2/S_1 at 250 and 300 eV shown in Table V.

E. Contributions of Other States

The reduced cross section $\rho_1(\tau, E)$ of Fig. 7 and the total cross section $S_1(E)$ derived from it represent charge-transfer transitions to states other than C and E. According to Table V, the C and E states together never amount to much more than 30% of the total charge transfer; a more conservative estimate, taking account of the uncertainty in properly locating the curve $\rho_1(\tau, E)$, is a maximum of 50% in the C and E states. At least 50% of the total charge transfer must then be attributed to other states, at energies above 65 eV.

We believe very little of this charge transfer ends in the ground state, $He(1s^2) + Ar^+(3p^5)$. If the molecular state $X^2\Sigma$ crosses $B^2\Sigma$ at all, it must do so at very small r and at high energies. Even the $A^2\Pi$ state will cross $B^2\Sigma$ at a rather small value of r, if the estimates in Fig. 1 are reasonably correct; in any case, the Σ-Π coupling will probably be too small to be important at these energies.

Even the curves $\rho_1(\tau, E)$ are not entirely devoid of structure. The pair of maxima that are seen at 140 eV appear to move apart at higher energies, and to move together and merge at lower energies. Not only do their relative positions move in a regular way, but the ratio between the first peak height and the succeeding valley bottom grows gradually as E increases (Table V). While this regularity may be an artifact in a curve that is probably a superposition of several states, we can subject the oscillations to the same analysis we have used for the C and E states. The results are shown in Fig. 12; most of the points for $N = 1$ are uncertain, since the second maximum is often weak and it is not clear its peak has truly been reached. If the regular pattern is accepted as real, there appears to be a structure with a threshold at

$$\tau_x \cong 1250 \text{ eV deg} = 0.8 \text{ a.u. rad},$$

whose average behavior is given by

$$a(\tau, E) \cong 0.064(\tau - 0.8) - 0.0041(\tau - 0.8)^2, \quad (39)$$

where the units are a.u. and rad; the slope gives us

$$\Delta b \cong 0.064 \text{ a.u.} - 0.0082(\tau - 0.8). \quad (40)$$

The first peak of the structure generally appears at about 2100 eV deg. This structure may represent the effect of a single crossing, and if so, its

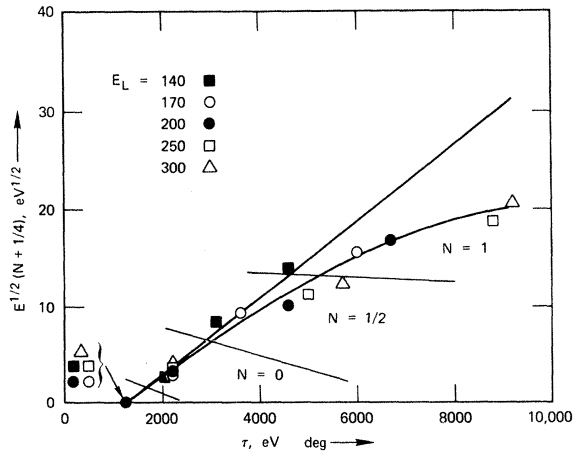

FIG. 12. Phase relations of the broad peak and valley structure included in $\rho_1(\tau, E)$. $(N+\frac{1}{4})E^{1/2}$ is plotted against τ.

total cross section may amount to 15–30% of S_1. However, we suspect that it is more likely to be the cumulative result of contributions from a number of crossings.

Assuming that the effective thresholds for the crossings creating this structure lie in a range of reduced angle between 1250 and 2100 eV deg, it is possible to estimate their locations. We assume a potential of the form of Eq. (3). The relationship between the threshold angle and the location of the crossing then depends on the energy loss ΔV_∞ in the final state. In Table VI we show the range of crossing locations corresponding to these various assumptions. Three values of ΔV_∞ have been chosen, corresponding respectively to the D state, the E state, and to an energy level of about 15 eV, in the middle of a region where a large number of excited states are available. The probable crossing distance falls roughly between 2.25 and 1.95 a.u. This agrees extremely well with a rough estimate based on the evidence of the elastic scattering measurements,[5] where a large drop in the elastic scattering was attributed to the opening of a considerable number of inelastic or charge-transfer channels, suggesting that many crossings occur in the region between 2.45 and 1.9 a.u.

From the data presented here, as well as from the elastic scattering results, it seems likely that a fairly large number of excited molecular states play a substantial part in the charge-exchange process at energies of 65 eV and above. Since the steep rise centered at about 1250 eV deg is prominent even in the data at 65 eV, a major fraction of the products must be metastable He atoms arising from curves dissociating at or above the E state. As Table VI shows, there are probably many states dissociating above the E state whose crossings with the B state lie below 25 eV, and these channels may be fully open at 65 eV.

F. Relations with Inelastic Scattering

The observations reported in this paper have a close connection with processes that should be observable in inelastic scattering. We have already suggested that the E state should be seen in inelastic scattering as well as in charge transfer. Furthermore, many of the other unidentified excited states that we assume to be collectively involved in the curve $\rho_1(\tau, E)$ are probably accompanied by inelastic channels at about the same dissociation energy. If that is the case, we would expect a number of inelastic channels to have thresholds in the region between 1250 and 2000 eV deg.

These expectations are confirmed by inelastic scattering measurements which will be published in a later paper.[6] Excitation of Ar to the configuration 4s occurs with a pattern of oscillations identical to those seen in the E-state charge transfer, except that the slow modulation as a function of energy is out of phase with that observed here. Inelastic scattering to a large number of higher excited states is also seen, with thresholds in the region of that shown by $\rho_1(\tau, E)$. Because of the possibility of energy analysis, the inelastic data provide still further information that can be used in elucidating further details of the potential-energy diagram for the system $HeAr^+$.

G. Connection with Recoil Scattering Measurements

Champion and Doverspike[23] have very recently reported the differential cross section at $E_L = 94$ eV for forward-scattered Ar^+, produced predominantly by endothermic processes with $\Delta E \geq 11$ eV, as a function of the recoil angle ω. Such energy losses may arise either from the production of excited He or excited Ar^+; spectroscopic evidence for the latter process exists,[24] and our results show that the former is also important.

It is particularly significant that they find a total cross section of about 0.9×10^{-16} cm^2 for scattering of fast Ar^+ ions in the forward cone out to 60°. This amounts to just about one-half of the total cross section as reported by Koopman[17] from a measurement of the production of slow Ar^+ ions. This has two consequences. On the one hand, Koopman's measurement of the total cross section may be too low by a factor of 1.5–2, because of discrimination against the fast Ar^+ (and Ar^{++}) ions; this would cause our normalization to be too low also. On the other hand, the process observed by Champion and Doverspike would be accompanied by a scattering of the neutral He produced by the reaction into angles larger than the 33° limit of our observations. The latter effect might cause our normalization to be too large, if we have underestimated the extrapolation of ρ to larger angles.

The Champion-Doverspike differential cross sections can be converted to the c.m. system if a single value of the energy loss ΔE is assumed. If $m_1 = m_{He}$, $m_2 = m_{Ar}$, and E_r = recoil energy, let

TABLE VI. Location r_x and crossing energy V_x of crossings to states other than C and E; dependence on energy loss ΔV_∞.

	$\tau_x = 1250$ eV deg		$\tau_x = 2100$ eV deg	
ΔV_∞ eV	r_x a.u.	V_x eV	r_x a.u.	V_x eV
8.43	2.27	12.6	2.01	20.0
11.05	2.21	14.0	1.98	20.9
15	2.14	15.9	1.93	22.8

us define

$$M = (1 + m_1/m_2)\,(m_2 E_r/m_1 E_L)^{1/2}, \tag{41}$$

$$N = (\Delta E/E_L)(1 - m_1/m_2). \tag{42}$$

In forward scattering, M is related to ω by the equation

$$M = \cos\omega + (\cos^2\omega - N)^{1/2}. \tag{43}$$

The c.m. scattering angle θ is then connected with ω by the relation

$$\tan\theta = M\sin\omega/(1 - M\cos\omega). \tag{44}$$

The recoil cross section $\sigma_r(\omega)$ and the c.m. cross section are related by

$$|\sigma_r(\omega)\sin\omega\, d\omega| = |\sigma_{c.m.}(\theta)\sin\theta\, d\theta|, \tag{45}$$

and it can be shown that

$$\left(\frac{d\omega}{d\theta}\right)_{\Delta E} = \frac{\cos\omega - M}{M}. \tag{46}$$

Thus, we can use the formula

$$\rho = \theta\sin\theta\,\sigma_{c.m.}(\theta) = \theta\sin\omega\,\sigma_r(\omega)(M - \cos\omega)/M \tag{47}$$

to convert Champion and Doverspike's cross sections to a reduced form comparable with ours.

We have made this conversion assuming two different values of ΔE, 11 and 19 eV; the results are shown in Fig. 13. The cross sections are not very sensitive to the assumption made about ΔE, and they compare reasonably well with our normalized results at $E_L = 100$ eV, although there is actually no overlap in the angular range covered. The trend of our curve suggests that our normalization is somewhat too large, but the two sets of data appear to agree to within a factor of 2. In view of the very large extrapolation involved in our normalization, this agreement is a lucky accident; furthermore, our detector at 100 eV discriminates in favor of He metastables, but the recoil measurement collects all the Ar^+ regardless of the final state of the He. This means that the normalization of the differential cross sections should be reduced by a factor of perhaps 2–4 at 100 eV, but they are probably more reliable at 300 eV. Although the quantities S_C and S_E of Table IV have been normalized in the same way, they are probably reasonable estimates of the total cross sections for charge transfer by way of the C and E states because of the compensating fact that they have been arrived at by integrating over only part of the angular range and over only the oscillating portions of the respective differential cross sections.

It is interesting to see an example where the charge-transfer scattering has been measured by one means or another over the entire angular range from 0 to 180° in the c.m. system.

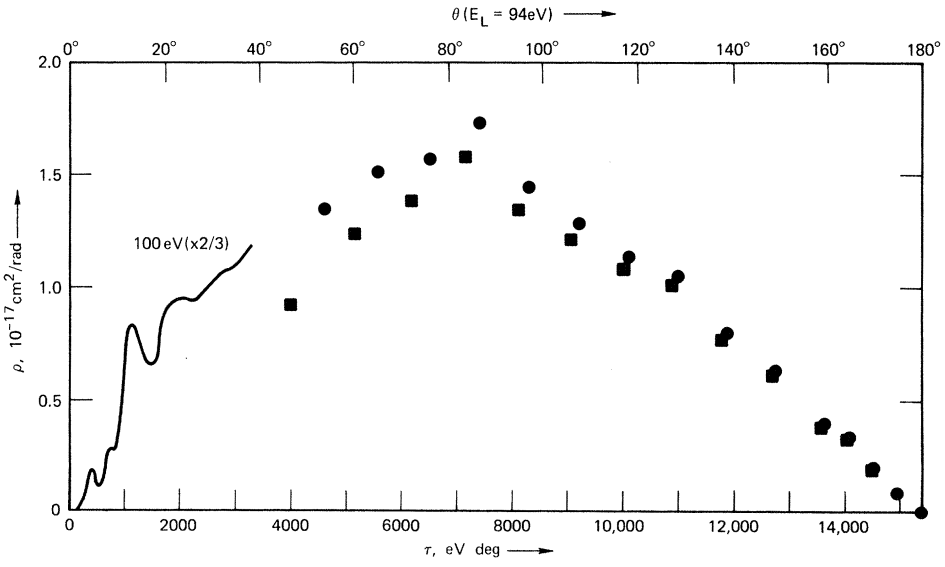

Fig. 13. Comparison of reduced cross sections from recoil scattering of Ar^+ and charge-transfer scattering of He. Solid circles: recoil data of Ref. 23 at $E_L = 94$ eV assuming $\Delta E = 11$ eV; solid triangles: same recoil data assuming $\Delta E = 19$ eV. Solid curve: data from Fig. 7 at $E_L = 100$ eV.

*Work at Stanford Research Institute supported by U. S. Atomic Energy Commission, Research Division.

†Formerly at Gulf General Atomic, San Diego, Calif. Experimental work in San Diego was supported by a

joint General Atomic-Texas Atomic Energy Research Foundation Program on controlled thermonuclear reactions.

‡Work at Cornell University was supported by a grant of the National Science Foundation.

§Now at Science Center, North American Rockwell, Thousand Oaks, Calif. 91360.

[1]M. Lipeles, R. Novick, and N. Tolk, Phys. Rev. Letters 15, 815 (1965).

[2]F. T. Smith, in *Atomic Physics*, edited by F. Bederson, V. W. Cohen, and F. M. J. Pichanick (Plenum, New York, 1969), p. 353.

[3]E. N. Fuls, P. R. Jones, F. P. Ziemba, and E. Everhart, Phys. Rev. 107, 704 (1957).

[4]W. Aberth and D. C. Lorents, Phys. Rev. 144, 109 (1966).

[5]F. T. Smith, R. P. Marchi, D. C. Lorents, W. Aberth, and O. Heinz, Phys. Rev. 161, 31 (1967).

[6]O. Bernardini, D. C. Lorents, and F. T. Smith (unpublished).

[7]For He_2^+, see G. Lockwood, H. Helbig, and E. Everhart, Phys. Rev. 132, 2078 (1963); D. C. Lorents and W. Aberth, *ibid.* 139, A1017 (1965); J. Baudon, M. Barat, and M. Abignoli, J. Phys. B1, 1083 (1968).

[8]For Ne_2^+, see P. R. Jones, T. L. Batra, and H. A. Ranga, Phys. Rev. Letters 17, 281 (1966).

[9]For Ar_2^+, see Ref. 4.

[10]For $NeAr^+$, see P. R. Jones, T. L. Batra, and H. A. Ranga, in *The Fifth International Conference on the Physics of Electronic and Atomic Collisions*, (Nauka, Leningrad, 1967), p. 470.

[11]D. Coffey, D. C. Lorents, and F. T. Smith, Phys. Rev. 187, 201 (1969).

[12]H. H. Fleischmann and R. A. Young, in Ref. 10, abstracts, p. 472.

[13]H. H. Michels (private communication); see Ref. 11.

[14]We use the concise designation of C. E. Moore, *Atomic Energy Levels*, Circular of the NBS No. 467 (U. S. GPO, Washington, D. C., 1949), for atomic configurations, for example, $Ar^+(3p^6) = (3s3p^6)$, $Ar^*(4s) = (3s^23p^44s)$, etc.

[15]J. A. Herce, K. D. Foster, and E. E. Muschlitz, Jr., Bull. Am. Phys. Soc. 13, 206 (1968); H. Hotop and A. Niehaus, *Sixth International Conference on the Physics of Electronic and Atomic Collisions* (MIT Press, Cambridge, Mass., 1969), p. 882; H. Hotop and A. Niehaus, Z. Physik 228, 68 (1969); H. Hotop, A. Niehaus, and A. L. Schmeltekopf, *ibid.* 229, 1 (1969).

[16]H. H. Fleischmann, R. A. Young, and J. W. McGowan, Phys. Rev. 153, 19 (1967); H. H. Fleischmann and R. A. Young, Phys. Rev. Letters 19, 941 (1967).

[17]D. W. Koopman, Phys. Rev. 154, 79 (1967).

[18]M. P. Utterback and D. H. Miller, Rev. Sci. Instr. 32, 1101 (1961).

[19]H. H. Fleischmann, R. A. Young, and J. W. McGowan, Phys. Rev. 153, 19 (1967).

[20]D. C. Lorents, W. Aberth, and V. W. Hesterman, Phys. Rev. Letters 17, 849 (1966); D. Coffey and D. C. Lorents (unpublished).

[21]W. R. Thorson and S. A. Boorstein, in *Fifth International Conference on the Physics of Electronic and Atomic Collisions* (Science Bookcrafters, Hastings-on-Hudson, N.Y., 1965), p. 218.

[22]F. T. Smith, in *Lectures in Theoretical Physics: Atomic Collisions Processes*, edited by S. Geltman, K. T. Mahanthappa, and W. E. Brittin, (Gordon and Breach, New York, 1969), Vol. XIC, p. 95.

[23]R. L. Champion and L. D. Doverspike, J. Phys. B2, 1353 (1969).

[24]D. Jaecks, F. J. DeHeer, and A. Salop, Physica 36, 606 (1967).